Medical Physics
The International Journal of Medical Physics Research and Practice

Liver segmentation for CT images using GVF snake

Fan Liu, Binsheng Zhao, Peter K. Kijewski, Liang Wang, and Lawrence H. Schwartz

Citation: Medical Physics **32**, 3699 (2005); doi: 10.1118/1.2132573
View online: http://dx.doi.org/10.1118/1.2132573
View Table of Contents: http://scitation.aip.org/content/aapm/journal/medphys/32/12?ver=pdfcov
Published by the American Association of Physicists in Medicine

Liver segmentation for CT images using GVF snake

Fan Liu,[a] Binsheng Zhao,[b] and Peter K. Kijewski[c]
Department of Medical Physics, Memorial Sloan-Kettering Cancer Center, 1275 York Avenue, New York, New York 10021

Liang Wang[d] and Lawrence H. Schwartz[e]
Department of Radiology, Memorial Sloan-Kettering Cancer Center, 1275 York Avenue, New York, New York 10021

(Received 4 February 2005; revised 3 October 2005; accepted for publication 6 October 2005; published 17 November 2005)

Accurate liver segmentation on computed tomography (CT) images is a challenging task especially at sites where surrounding tissues (e.g., stomach, kidney) have densities similar to that of the liver and lesions reside at the liver edges. We have developed a method for semiautomatic delineation of the liver contours on contrast-enhanced CT images. The method utilizes a snake algorithm with a gradient vector flow (GVF) field as its external force. To improve the performance of the GVF snake in the segmentation of the liver contour, an edge map was obtained with a Canny edge detector, followed by modifications using a liver template and a concavity removal algorithm. With the modified edge map, for which unwanted edges inside the liver were eliminated, the GVF field was computed and an initial liver contour was formed. The snake algorithm was then applied to obtain the actual liver contour. This algorithm was extended to segment the liver volume in a slice-by-slice fashion, where the result of the preceding slice constrained the segmentation of the adjacent slice. 551 two-dimensional liver images from 20 volumetric images with colorectal metastases spreading throughout the livers were delineated using this method, and also manually by a radiologist for evaluation. The difference ratio, which is defined as the percentage ratio of mismatching volume between the computer and the radiologist's results, ranged from 2.9% to 7.6% with a median value of 5.3%. © *2005 American Association of Physicists in Medicine*. [DOI: 10.1118/1.2132573]

Key words: liver contour, image segmentation, GVF, snake, edge map, CT

I. INTRODUCTION

Computed tomography (CT) of the liver is the most frequently used diagnostic modality to screen the liver in patients with malignancy. Liver segmentation is helpful in the automatic detection and definition of focal lesions. It is also critical in planning presurgical operations for hepatic resection and assessing therapy response. Computer-aided liver segmentation is a challenging task because of the complex structure of the abdomen. Several organs adjacent to the liver, for instance, stomach, kidney, and heart, may have densities similar to that of the liver. The boundaries between such organs and the liver can thus be weak, making separation of the liver using computer algorithms more difficult. Moreover, lesions residing at the liver edges often lead to an incomplete extraction of the liver parenchyma.

A number of automatic and semiautomatic methods for segmentation of the liver have been developed.[1–7] These methods can be classified into region-based and boundary-based approaches. The region-based approach applies thresholds determined either by analyzing the image histogram or a small portion of the liver to obtain an initial area approximating the liver, which is then refined into the actual liver.[1–4] For the boundary-based methods, a fractional Brownian motion model and a visible human model have been proposed to extract the initial liver contours or models. These initial contours or models are then refined by deformable models.[5,6] To our best knowledge, these methods fail to completely overcome the difficulties in the liver segmentation mentioned.

Originally introduced by Kass, the snake algorithm seeks a balance between the internal energy and external energy, where the internal energy reflects the snake's tension and rigidity; and the external energy attracts the snake to deform toward an edge. The snake has the properties of continuity and smoothness in delineating boundaries, thus making it a powerful tool for image segmentation.[8] However, the traditional snake has two major difficulties. One is the narrow capture range, which requires an initial curve close to the real edge, and the other is the difficulty in delineating concave boundaries.[9] There have been different solutions proposed to solve these problems, such as the gradient vector flow (GVF) snake,[9–12] multiresolution methods,[13] pressure forces,[14] distance potentials,[15] and control points.[16] Among these methods, the GVF snake is superior as its external force, i.e., the GVF field, has large values at edges and varies slowly in homogeneous regions. In this way it can enlarge the capture range. It can also force the snake to deform into concave edges.[9–12]

In our previous work, we applied a snake with a gradient vector flow field (GVF snake) for the automatic delineation of the normal liver on two-dimensional (2D) images.[7] An edge map was computed using the Canny edge detector, unwanted edges inside the liver were removed using a liver

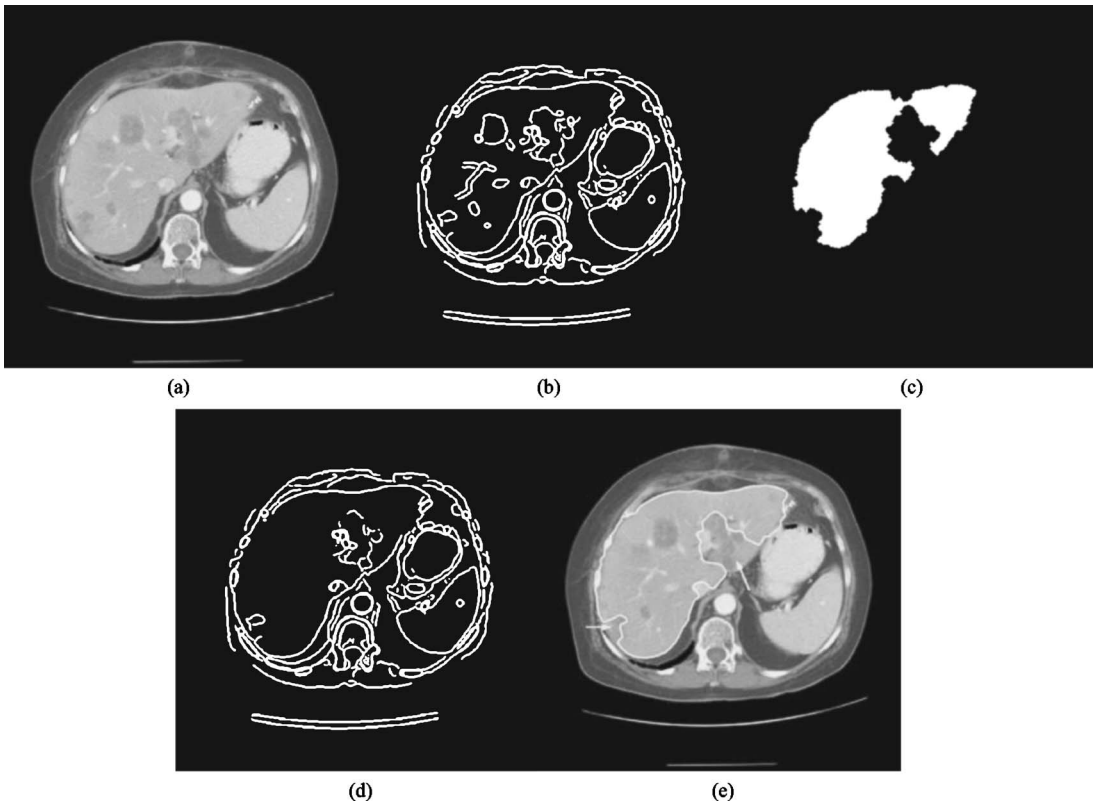

FIG. 1. Difficulties in using our previous method. (a) Original image. (b) Initial edge map obtained using the Canny edge detector. (c) The liver template. (d) Edge map modified by the liver template. (e) The final result (white contour) does not include lesions residing at the liver edge, as indicated by the arrows.

template, and an initial contour was formed automatically and subsequently refined by the GVF snake to obtain the final liver contour. We found that the snake could keep the liver contour continuous and smooth, and it delineated liver boundaries even when they were weak. The GVF field could not only help identifying an initial liver contour that was within the capture range of the snake, but also prevented the snake from leaking into the surrounding tissues with densities similar to liver. We obtained promising preliminary results with the automatic delineation of the normal liver.[7] However, if the liver has lesions at the boundary, our previous method may fail to include them in the liver. Figure 1 shows such an example. The liver template [Fig. 1(c)], which is the largest object in the image with an upper and lower threshold applied, roughly represents the liver, but may exclude the lesions whose densities do not fall into the density range defined by the two thresholds. Those edges of such lesions may prevent the GVF snake from approaching the actual liver boundary [Fig. 1(e)].

In this study we have improved the liver delineation algorithm by developing a concavity removal algorithm that aims to deal with abnormal livers, particularly with those having lesions at the liver edges. We have also extended the 2D algorithm to a three-dimensional (3D) algorithm in a slice by slice fashion.

II. METHODS

A flow chart of the method developed for the extraction of 2D liver contours is shown in Fig. 2. The algorithm consists

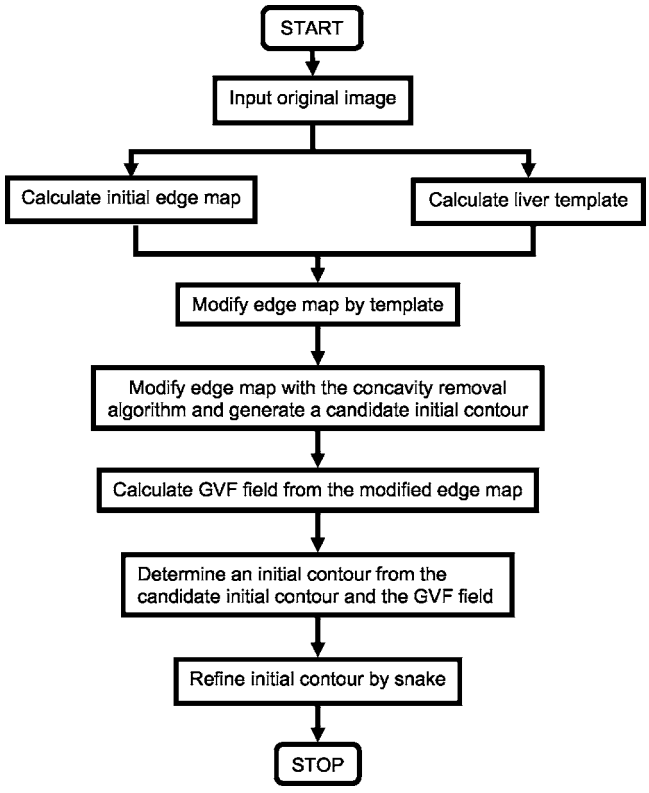

FIG. 2. Flow chart illustrating the method developed to delineate the liver contours.

of the following steps: (1) Calculate an initial edge map using the Canny edge detector and estimate a liver template. (2) Modify the initial edge map by suppressing the edges inside the liver with the liver template. (3) Further modify the edge map with a concavity removal algorithm based on an assumption of the liver shape, and generate a candidate initial liver contour. (4) Compute the GVF field based on the modified edge map. (5) Determine the initial liver contour by jointly considering the candidate initial contour and the computed GVF field. (6) Deform the initial contour into the actual liver contour using the snake.

A. Edge map

1. Initial edge map

The Canny edge detector was chosen to estimate an initial edge map because of its ability to define a ridge at the boundary of the liver with a uniform height, even for cases where density differences between the liver and adjacent structures may vary substantially.[17] The variations are typically caused by partial volume effects, image noise, or varying contrast of the liver relative to its adjacent structures.

Parameters used in the Canny edge detector are a lower threshold, an upper threshold, and a standard deviation for a Gaussian filter. The two thresholds are applied to determine the edges and the Gaussian filter to reduce noises in the image. To emphasize the main edges in an image, the two thresholds should be large; and to find the details of an image, their value should be small. A larger standard deviation should be used for a noisy image. However, a standard deviation that is too large may blur the image as well as the edges. In our study the parameters of the Canny edge detector were defined as 0.12, 0.05, and 2 for the high threshold, low threshold, and standard deviation, respectively. Figure 1(b) shows an example of the edge map derived by the Canny edge detector.

2. Liver template

As shown in Fig. 1(b), there are other edges both within and outside the liver. Edges inside the liver can prevent the GVF snake from approaching the liver boundary and therefore need to be suppressed. This is done with a liver template.[7] The original images are preprocessed by a median filter with a size of 21×21 pixels so that a clear and sharp peak representing the liver can be formed in the histogram of the filtered image. By analyzing the histogram, two thresholds, one at each side of the liver peak, can be identified to generate a binary volume image. The voxels are set to one in the binary images if their densities in the original image are between the two thresholds. All 3D objects in the binary image are identified by a six-connection neighborhood and the one with the largest volume is identified as the liver template.

Holes in each slice of the template are filled, and the template is smoothed morphologically by eroding with a disk with a radius of three pixels. The advantage of using a volume to generate the liver template lies in its ability to localize the liver in each slice, even if the liver section is small in the slices towards the superior or inferior parts of the liver.

3. Concavity removal algorithm

As shown in Fig. 1, a liver may have lesions at its boundary. Often, such lesions cannot be included into the liver template [Fig. 1(c)], and their edges will prevent the GVF snake from approaching the liver boundary [arrows in Fig. 1(e)]. To remove the concave segments in the liver contour caused by the lesions [Fig. 1(e)], a concavity removal algorithm was developed to further modify the edge map prior to application of the GVF snake. The concavity removal algorithm is based on the assumption that a liver contour is mostly convex with some relatively shallow concave boundary segments.

As shown in Fig. 1(d), the liver edge may not be continuous on the edge map. To correct this problem the following two steps are performed. First, the edge segments are thickened iteratively by morphological dilation until a closed stripe surrounding the liver is formed [Fig. 3(a)]. The structure element used in the dilation is a disk with radius of three pixels. Second, the region surrounded by the stripe is dilated $n-1$ times using the same structure element, where n is the number of dilations in the first step. The boundary of the region is extracted as a candidate initial liver contour [dotted line in Fig. 3(b)].

The concavity removal algorithm is illustrated in Fig. 4. A concavity segment is determined by identifying two turning points, which are defined as the points that separate the concave and convex segments [points A and B in Fig. 4]. The depth of a concave segment is defined as the ratio of the segment length ($curve_{AB}$) to the distance between its two ending points ($line_{AB}$). If a concavity depth is greater than a predefined threshold, the segment will be replaced by a straight line [dotted line in Fig. 4]; otherwise, it will be retained. The smaller the threshold, the stricter the criteria for the concavity removal. In the extreme case of a threshold equal to one, any concavity will be removed no matter how shallow it is.

The posterior and left part of a liver contour has a more complex shape than the anterior and right part; the former has concavity segments, whereas the latter appears almost convex. The two parts are adaptively identified by the top and bottom points of the contour in the image, where the left (anatomical) segment between the two extreme points is classified as the posterior and left part, and the right segment the anterior and right part. To improve the accuracy of identification of the concavity segments, a stricter criterion is applied to the anterior and right part of the liver contour. A lower value of the threshold (1.05) is defined for the anterior and right part of the liver contour, while a higher value of the threshold (1.2) of the depth parameter is defined for the posterior and left part of liver contour

After applying the concavity removal algorithm, a new contour is formed [solid line in Fig. 3(b)]. The edge map is then modified by removing all edges that are inside the new contour [Fig. 3(c)]. The process, from thickening the edges

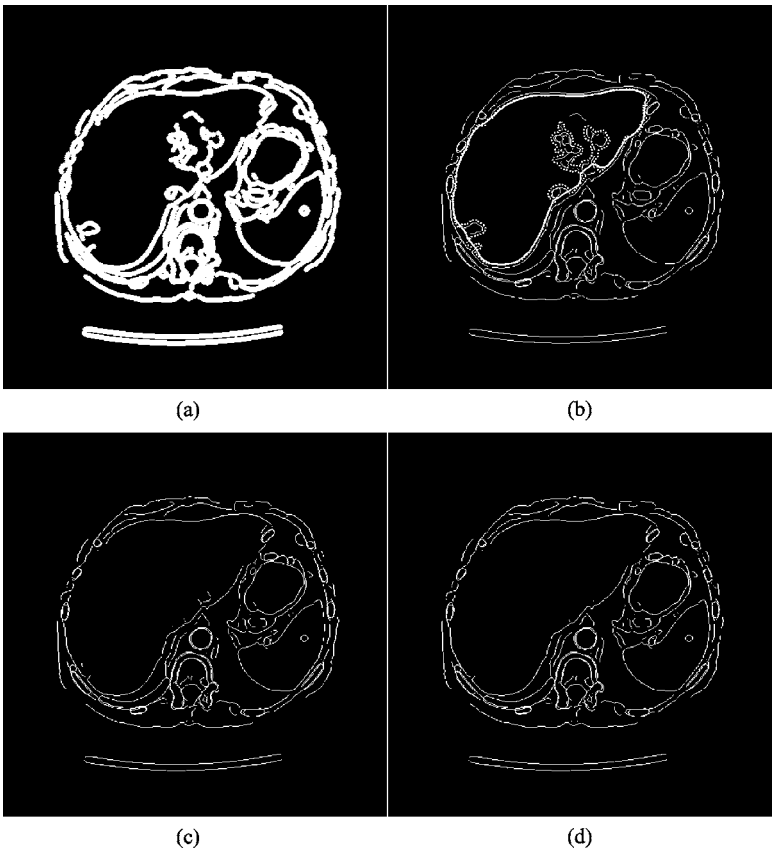

FIG. 3. Illustration of edge map modification by the concavity removal algorithm. (a) Thickened edge map. (b) Contour modification. The liver contour (dotted line) is modified to form a new contour (solid line). (c) Edges inside the new contour in (b) are removed. (d) After several iterations, the final edge map can be formed.

to removing edges inside the new contour, is repeated until all edges inside the liver are removed. Figure 3(d) shows the final edge map.

B. GVF field and initial contours

Based on the final edge map, the computation of the GVF field can be carried out by solving the following equations:[9–12]

$$\eta\nabla^2 u - (u - f_x)(f_x^2 + f_y^2) = 0, \tag{1}$$

$$\eta\nabla^2 v - (v - f_y)(f_x^2 + f_y^2) = 0, \tag{2}$$

where $[u(x,y), v(x,y)]$ are the two components of the GVF field $w(x,y)$, η is a constant weight, ∇^2 is the Laplacian operator, f is the edge map, and f_x and f_y are partial derivative of f with respect to x and y, respectively. The value of η depends on the noise in the edge map (the more noise, the larger η).[9] Since the edges inside the liver are removed in the edge map, the value of η is not sensitive to different cases. Given the digital matrices u, v, and f, the partial derivative and Laplacian operator computations are implemented by differences. Equations (1) and (2) can be solved iteratively. The weight η is set as 0.2, and the iteration is performed 50 times. Since the magnitude of GVF field in each point is usually small, it is enhanced by normalization as proposed by Xu.[18]

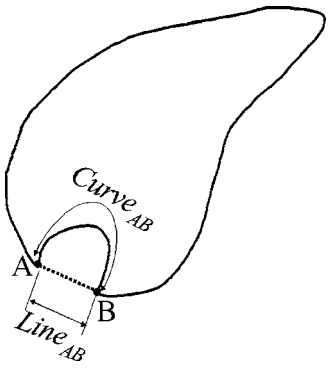

FIG. 4. Concavity removal algorithm. The concavity depth is defined as the ratio of the segment length to the length of the straight line, i.e., $curve_{AB}/line_{AB}$. If it is larger than a predefined threshold, the concavity is replaced by the straight dotted line AB.

Due to finite number of iteration steps, as well as the removal of the edges inside the liver, there is no GVF field in the center part of the liver [Fig. 5(a)]. In our previous work, the initial liver contour was the contour of the empty region of the GVF field.[7] We found that the candidate initial contour generated by the previous concavity removal step may be closer to the final liver edge than the (initial) contour of the empty region in the GVF field. However, there is no guarantee that the candidate initial contour is fully within the GVF field. In this study, the candidate initial contour obtained in

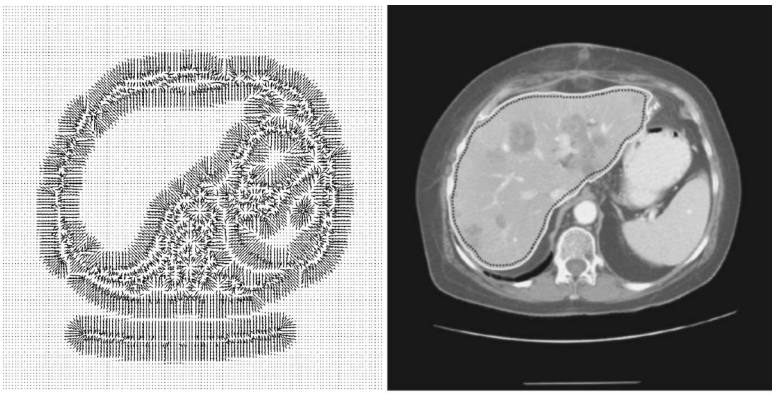

(a) (b)

FIG. 5. Liver contour delineation by GVF snake (a) GVF field estimation from the modified edge map after 50 iterations (subsampled by a factor of 4). (b) The original image overlapped with the initial contour (black dots) and the final contour (white solid).

the previous concavity removal step and the contour of the empty region of the GVF field are jointly considered to identify the initial liver contour. This is done by merging the two regions encircled by these two contours and extracting the border of the combined regions as the new initial contour. This will ensure that the initial contour is within the GVF field and as close as possible to the liver edge.

C. Liver contour delineation

The initial contour is then deformed by the snake to refine the liver boundary [Fig. 5(b)]. The implementation of the snake is done by solving the following equation:

$$\alpha \mathbf{x}''(s) - \beta \mathbf{x}''''(s) + \mathbf{w} = 0, \tag{3}$$

where $x(s)=[x_1(s),x_2(s)]$ is the snake defined on interval [0, 1]; α and β are weights that control the snake's tension and rigidity, respectively; $x''(s)$ and $x''''(s)$ denote the second and fourth derivatives of $x(s)$ with respect to s. Equation (3) can be solved in an iterative way.[8,9,12]

Usually the values of α and β need adjustment if an edge map is noisy, or an edge has a zigzag shape. In this study, however, the edges inside the liver are removed, and the liver edges are smooth. Therefore, the final result is not sensitive to the choice of values for these parameters. The values of these parameters are taken as 0.6 and 0.01, which were determined experimentally.

Often, the initial contour is close to the final contour as it is derived from the liver edge map. However, due to morphological operations, some tips of the liver edges may not be restored by the initial contour without the snake [Fig. 6(g)]. Thus the GVF snake is applied to obtain a more accurate liver contour.

D. Segmentation of the liver volume

The 2D algorithm can be extended to segment the liver volume in a slice by slice manner. For convenience, the slice to be segmented is called the current slice, and the adjacent segmented slice is called previous slice.

A starting slice is manually selected on which the liver has a large area profile and the segmentation result is accurate. The reason is that the starting slice will be used as a mask to eliminate edges far beyond the liver in its adjacent slices, so the large profile of the liver in the starting slice will ensure that no liver edges will be eliminated.

Figure 6 demonstrates the slice by slice procedure. The contour of the previous slice [dotted line in Fig. 6(c)] is used to form an area mask. The mask will then be anisotropically dilated using a structure element [inset of Fig. 6(c)]. The structure element is so chosen to allow a larger expansion towards the faster changing direction of the liver between slices.

The dilated mask is applied to suppress edges beyond the liver in the initial edge map [Fig. 6(b)] of the current slice. Then the liver template [Fig. 6(d)] is applied to suppress edges inside the liver in the masked edge map [Fig. 6(e)]. After that, the edge map modification by the concavity removal algorithm, GVF field computation, initial contour generation, and snake refinement follow the same way as described previously [Figs. 6(f) and 6(g)].

The suppression of edges beyond the liver by the mask is important in the segmentation of the current slice. For example, if the stomach has similar densities to the liver [Fig. 6(a)], the edges between them are weak and could not be detected by the Canny edge detector [Fig. 6(b)]. Moreover, the liver template may leak into the stomach due to their similar densities [Fig. 6(d)]. So there may be no edges between the liver and the stomach in the edge map [Fig. 6(e)], and the snake will leak into the stomach if the edges of the stomach are not eliminated by the mask [Fig. 6(h)].

The mask can also improve algorithm's efficiency. Because no edge exists outside the mask, the GVF computation can be limited within the smallest rectangle that contains the mask.

E. Evaluation of the method

To evaluate the accuracy of the method, the computer generated results were compared with an independent radiologist's manual result, although multiple observers' results are more helpful for the evaluation.[19] To ignore minor discrepancies between the manual results and the computer generated liver contour, only the mismatching regions beyond a ±3 mm ring surrounding the manual results on each slice

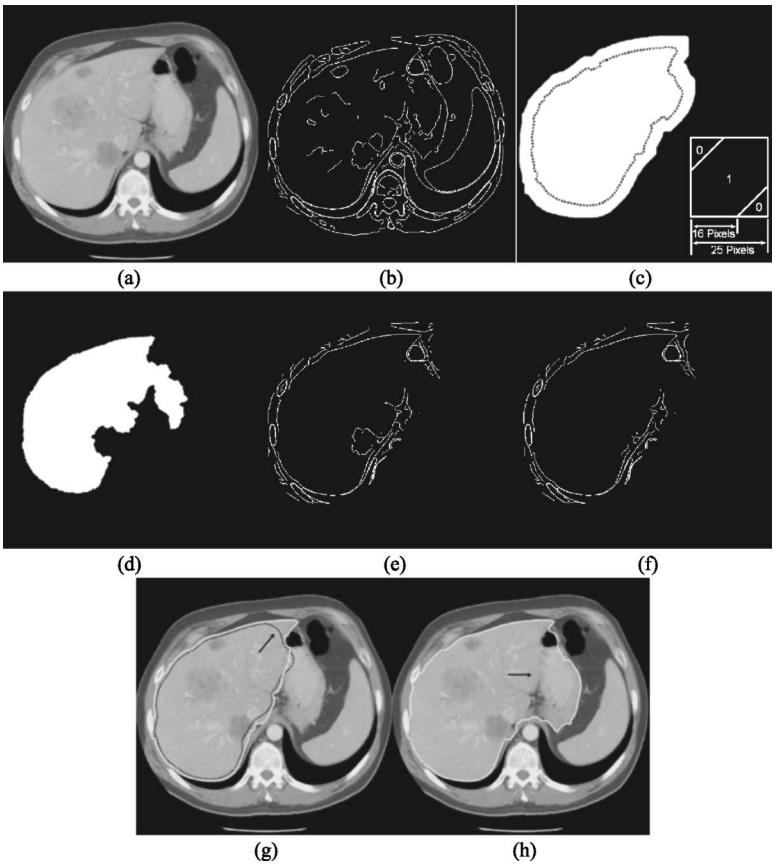

FIG. 6. Illustration of the segmentation of the liver volume. (a) Original image to be segmented. (b) Initial edge map. (c) Mask obtained by dilating the result from the segmented liver (black dotted contour) in the previous slice using the structure element shown at the right lower corner. (d) The liver template. (e) Edge map after modification by the mask and the liver template. Some edges of the lesion and fissure remain inside the liver. (f) Final edge map after modification by the concavity removal algorithm. There is no edge within the liver. (g) The original image overlapped with the final contour (white solid). It also shows the initial contour refined by the snake algorithm (arrow). (h) The GVF snake may leak into stomach if no mask is applied (arrow).

were considered to be an error. The difference ratio is defined as the total number of mismatching voxels divided by the total number of voxels for the manual result.

III. EXPERIMENTAL RESULTS AND DISCUSSIONS

Twenty contrast enhanced volumetric liver images (551 2D liver slices) were selected from a previous study on liver colorectal metastases. Cases were selected with multiple large lesions spread throughout the livers (1–28 lesions per case, median 9) and with lesions residing at the liver edge to develop and evaluate our algorithm. The dimensions of all slices are 512×512 pixels. The in-plane pixel size ranges from 0.56 mm $\times$ 0.56 mm to 0.87 mm $\times$ 0.87 mm. The slice thicknesses are 3.75, 5.0, 7.0, and 7.5 mm. These thicknesses were chosen for our study because they were available, and this range of slice thickness is widely used in oncology in current clinical practice.

A radiologist manually delineated each of the 551 2D liver images using our research PACS system.[20] Computer results were then compared with the radiologist's manual results.

Since the CT images are digital images with various resolutions, we cannot draw a ring around the radiologist results at a width of exactly ±3 mm. To overcome this difficulty, we calculated the error ratios at different widths and then interpolated the error ratio at ±3 mm. The median value of the difference ratios was 5.3% with the maximum and minimum value of 7.6% and 2.9%, respectively.

Errors in the computer results occurred mainly at heart, liver porta, lesions not forming concavities, and gall bladder.

In the superior part of the liver the heart may appear next to the liver. Due to the partial volume effect on some slices, even the radiologist had difficulty separating the heart from the liver. In such situation a large error could occur. There are 90 slices with heart next to liver, among which 13 slices contain such errors. Almost all such leakages occur for cases with slice thickness of 7.5 mm, except one with a slice thickness of 3.75 mm. Although only 20 cases were tested, this kind of error may be expected to be reduced with a thinner slice thickness.

If a lower density gall bladder is present on a slice, our algorithm might falsely flatten the concavity segment caused by the gall bladder and include it in the result. In the 56 slices where gall bladders are adjacent to the livers, 20 were included in the computer results. For the same reason, most liver portaes were easily identified by our algorithm as concavities and were included as part of the liver. If a lesion does not form a deep concavity on the liver boundary, say, at a corner of the liver, its edges may not be flattened by the concavity removal algorithm and the lesion therefore will be excluded from the liver. There are 367 slices having lesions, among which 65 have lesions that are excluded, although most of the lesions are small. Although changing the thresholds of the concavity removal algorithm will definitely include more lesions in the results, the 3D liver shape infor-

mation may be more useful in further improving our algorithm in reducing all the errors mentioned earlier.

The algorithm used several sets of parameters. The values of the parameters were determined experimentally. However, for extreme cases, for example, images with lower contrast enhanced effects due to the fat in the liver, some manual adjustments were necessary. The difficulty lies in the determination of the parameters for the liver template and Canny edge detector when the liver densities were too close to those of the adjacent organs or the lesions are too big (e.g., occupying more than half of the liver in some slices). Six cases required parameter adjustments, among which three adjustment were for the template computation, and the other three for the Canny edge detector. Although all the images were contrast enhanced, the three cases had very poor contrast or had such big lesions that occupied more than half of liver region in some slices, and thus made the parameter adjustments necessary for template computation. The other three cases that the parameters for the Canny edge detector were adjusted shared a common feature that they had very large lesions occupying one third to more than a half of liver regions in some slices. Those lesions were also at liver corners in those slices. To include such big lesions in the liver, we had to adjust the parameters of the Canny edge detector. The parameters used in concavity removal algorithm and the GVF snake computations were fixed for all cases in this study.

One radiologist manually drew the liver contour once, so the inter- and intro-observer variations, as well as the effect of the window/level applied to delineating the contours were not considered in evaluating the method. We plan to study such effects in the future study. As a compensation, the ring surrounding the radiologist's result is applied to neglect minor discrepancy between the manual results and the computer generated results, thus emphasizing the major errors in the computer results. The width of 3 mm is determined by the observation that no big errors are excluded and minor discrepancies between computer results and manual results are ignored.

The experiments did not consider the effects of different CT scanners and different CT imaging parameters. Furthermore, a limited number of 20 cases was used to develop and test the algorithm. A thorough evaluation of the method including optimizing the parameters using more cases is required. It is possible that some of the parameter values could be different than they are now after further study.

The cases used for analysis in this article were particularly difficult ones. All patients had hepatic metastases and were deemed potential candidates for surgical resection. The CT scans were obtained for preoperative evaluation and staging. All of the 20 cases had lesions in or near liver edges and a high proportion of patients (85% of the 20 cases) had multiple heterogeneous liver masses. Therefore, this data represents a "worst case scenario." In a general patient population, even in a general oncology population, it is unlikely to encounter as many lesions, as large lesions or contour deforming lesions. The goal in this evaluation was to test the algorithm under these "adverse" conditions.

The utility of this algorithm will greatly enhance radiologists and technologist productivity by providing a tool which may semi-automatically segment the liver in a large portion of cases and slices. It is not anticipated that the algorithm will work in all cases and on all slices, however the alternative of manual liver delineation is for more time consuming.

IV. CONCLUSION

We have developed a GVF snake method to semiautomatically segment liver volumes on contrast enhanced CT images. The method has been designed to improve the delineation of low contrast anatomy between the liver and the surrounding tissues (e.g., stomach, kidney) as well as identification and inclusion of lesions at the liver boundaries. Differences by volume between the segmentation results obtained by the computer method and a radiologist ranged from 2.9% to 7.6% with a median value of 5.3%.

[a]Electronic mail: liuf@mskcc.org
[b]Electronic mail: zhaob@mskcc.org
[c]Electronic mail: kijewskp@mskcc.org
[d]Electronic mail: wang6@mskcc.org
[e]Electronic mail: schwartl@mskcc.org

[1]L. A. Farjo, D. M. Williams, P. H. Bland, I. R. Francis, and C. R. Meyer, "Determination of liver volume from CT scans using histogram cluster analysis," J. Comput. Assist. Tomogr. **16**, 674–683 (1992).
[2]K. T. Bae, M. L. Giger, C. Chen, and C. E. Kahn, Jr., "Automatic segmentation of liver structure in CT images," Med. Phys. **20**, 71–78 (1993).
[3]L. Gao, D. G. Heath, B. S. Kuszyk, and E. K. Fishman, "Automatic liver segmentation technique for three-dimensional visualization of CT data," Radiology **201**, 359–364 (1996).
[4]J. Hong, T. Kaneko, R. Sekiguch, and K. Park, "Automatic liver tumor detection from CT," IEICE Trans. Inf. Syst. **E84-D**, 741–748 (2001).
[5]E. Chen, P. Chung, C. Chen, H. Tsai, and C. Chang, "An automatic diagnostic system for CT liver image classification," IEEE Trans. Biomed. Eng. **45**, 783–794 (1998).
[6]L. Soler, H. Delingette, G. Malandain, J. Montagnat, N. Ayache, C. Koehl, O. Dourthe, B. Malassagne, M. Smith, D. Mutter, and J. Marescaux, "Fully automatic anatomical, pathological, and functional segmentation from CT scans for hepatic surgery," Comput. Aided Surg. **6**, 131–142 (2001).
[7]F. Liu, B. Zhao, P. Kijewski, M. S. Ginsberg, L. Wang, and L. H. Schwartz, "Automatic liver contour segmentation using GVF snake," Proc. SPIE **5370**, 1466–1473 (2004).
[8]M. Kass, A. Witkin, and D. Terzopoulos, "Snakes: Active contour models," Int. J. Comput. Vis. **1**, 321–331 (1987).
[9]C. Xu, "Deformable models with application to human cerebral cortex reconstruction from magnetic resonance images," Dissertation, 2000.
[10]C. Xu and J. L. Prince, "Gradient vector flow: A new external force for snakes," IEEE Proc. Conf. on Comp. Vis. Patt. Recog. (CVPR'97), 1997, pp. 66–71.
[11]C. Xu and J. L. Prince, "Snakes, shapes, and gradient vector flow," IEEE Trans. Image Process. **7**, 359–369 (1998).
[12]C. Xu, D. L. Pham, and J. L. Prince, "Medical image segmentation using deformable models," *Handbook of Medical Imaging* (SPIE, Bellingham, WA, 2000), Vol. 2, pp. 129–174.
[13]B. Leroy, I. Herlin, and L. D. Cohen, "Multi-resolution algorithms for active contour models," Proceedings of the 12th International Conference on Analysis and Optimization of Systems Images, Wavelets and PDE'S, Rocquencourt (France), 1996, pp. 58–65.
[14]L. D. Cohen, "On active contour models and balloons," CVGIP: Image Understand. **53**, 211–218 (1991).
[15]L. D. Cohen and I. Cohen, "Finite-element methods for active contour models and balloons for 2-D and 3-D images," IEEE Trans. Pattern Anal. Mach. Intell. **15**, 1131–1147 (1993).
[16]C. Davatzikos and J. L. Prince, "An active contour model for mapping the cortex," IEEE Trans. Med. Imaging **14**, 65–80 (1995).

[17]J. Canny, "A computational approach to edge detection," IEEE Trans. Pattern Anal. Mach. Intell. **PAMI-8**, 679–698 (1986).
[18]C. Xu and J. L. Prince, "Active contours, deformable models, and gradient vector flow," 2005, available online at http://iacl.ece.jhu.edu/projects/gvf/, accessed on Oct. 3, 2005.
[19]V. Chalana and Y. Kim, "A methodology for evaluation of boundary detection algorithms on medical images," IEEE Trans. Med. Imaging **16**, 642–652 (1997).
[20]J. Kalaigian, L. Bidaut, B. Zhao, P. K. Kijewski, and L. H. Schwartz, "Design and implementation of a flexible PACS interface for clinical research applications," 88th Scientific Assembly and Annual Meeting, RSNA 2002, Chicago, Illinois.